HI tomographic imaging of the Cosmic Dawn and Epoch of Reionization with SKA

Garrelt Mellema[*],[1] **León Koopmans,**[2] **Hemant Shukla,**[3] **Kanan K. Datta,**[4] **Andrei Mesinger**[5]**, Suman Majumdar**[1] **on behalf of the CD/EoR Science Working Group**
[a]*Dept. of Astronomy & Oskar Klein Centre, Stockholm University, AlbaNova, SE-10691*
Stockholm, Sweden; [b]*Kapteyn Astronomical Institute, Universiity of Groningen, P.O. Box 9000,*
9700 AA Groningen, The Netherlands; [c]*Astronomy Centre, Department of Physics & Astronomy,*
Pevensey II Building, University of Sussex, Falmer, Brighton BN1 9QH, UK; [d]*National Centre*
For Radio Astrophysics, Post Bag 3, Ganeshkhind, Pune 411 007, India; [e]*Scuola Normale*
Superiore, Piazza dei Cavalieri 7, I-56126 Pisa, Italy
E-mail: garrelt@astro.su.se

We provide an overview of 21cm tomography of the Cosmic Dawn and Epoch of Reionization as possible with SKA-Low. We show why tomography is essential for studying CD/EoR and present the scales which can be imaged at different frequencies for the different phases of SKA-Low. Next we discuss the different ways in which tomographic data can be analyzed. We end with an overview of science questions which can only be answered by tomography, ranging from the characterization of individual objects to understanding the global processes shaping the Universe during the CD/EoR.

---

[*]Speaker.

---

1. Introduction

SKA1-Low will provide enough sensitivity to deliver an image signal to noise larger than 1 for signals of order 1 mK on scales of a few arcminutes for a combination of bandwidth and integration time $Bt \approx 1000$ MHz hrs. This capability allows imaging of the redshifted 21cm signal from the Epoch of Reionization on these angular scales. SKA1-Low will be the first interferometer that will be able to do this as the precursors LOFAR, MWA and PAPER have at least an order of magnitude less sensitivity and thus can only hope to characterize the signals statistically, for example through the value of the 21cm power spectrum at certain scales or the variance of the signal at all observable scales or higher-order statistics such as skewness and kurtosis.

This chapter which forms part of the set of chapters from the Cosmic Dawn/Epoch of Reionization section of this volume discusses this imaging capability of SKA1-Low and how it can be used to improve our understanding of these two epochs.

Actually as first discussed in some detail by Madau et al. (1997), since the signal can be imaged in many adjacent frequency bins, it is better to speak of 21cm *tomography* when analysing the stacks of images, or image cube, at different frequencies. The frequency direction is of course special as along this line-of-sight direction the signal is seen from different look back times ('light cone effect') and also is affected by redshift space distortions introduced by the peculiar velocity field of the gas. Still, the three-dimensional data will provide a measurement of the distribution of the 21cm signal in three-dimensional space. In this the 21cm signal is more akin to galaxy redshift surveys at very much lower redshifts and very different from the Cosmic Microwave Background which only provides us with a snapshot from a single epoch.

The 21cm signal also differs in another fundamental way from the CMB signal. Whereas the CMB fluctuations reflect the tiny density fluctuations around the time of decoupling, the 21cm signal has strongly non-linear fluctuations. Furthermore, whereas the CMB fluctuations follow a Gaussian distribution and thus are statistically fully described by a power spectrum analysis, the same is not true for the 21cm signal whose probability distribution function (PDF) has been shown to be strongly non-Gaussian (Mellema et al. 2006). So, although a power spectrum analysis can reveal important properties of the signal, it does not fully describe it. This is illustrated in Fig. 1 which shows a 21cm image derived from a full numerical simulation of reionization and an image with the same power spectrum but a Gaussian PDF. The two images are very different but at the same time are indistinguishable in a power spectrum analysis.

2. The 21cm signal & sources of variations

As for the example described in more detail in Furlanetto et al. (2006), the redshifted 21cm signal from the intergalactic medium during the CD/EoR is the differential brightness temperature $\delta T_{\rm b}$ which when scaled to canonical values can be written as

$$\delta T_{\rm b} \approx 27 x_{\rm HI}(1+\delta) \left(\frac{1+z}{10}\right)^{\frac{1}{2}} \left(1 - \frac{T_{\rm CMB}(z)}{T_{\rm s}}\right) \left(\frac{\Omega_{\rm b}}{0.044}\frac{h}{0.7}\right) \left(\frac{\Omega_{\rm m}}{0.27}\right)^{\frac{1}{2}}$$

$$\left(\frac{1-Y_{\rm p}}{1-0.248}\right) \left(1 + \frac{1}{H(z)}\frac{{\rm d}v_{\parallel}}{{\rm d}r_{\parallel}}\right)^{-1} \quad {\rm mK}, \tag{2.1}$$
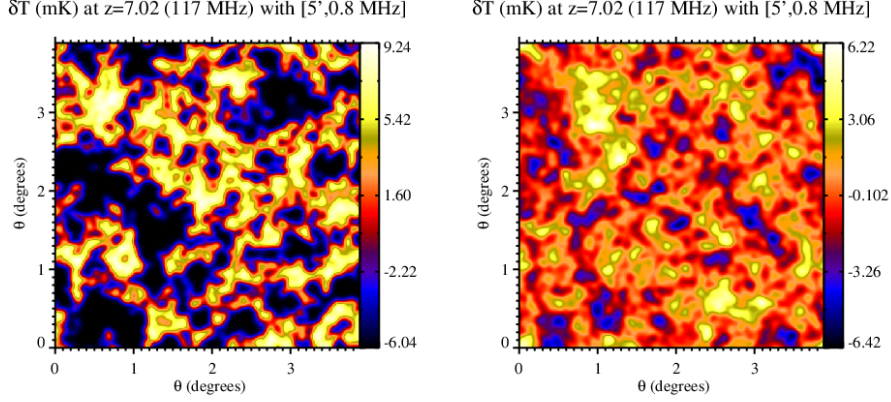
Figure 1: Left panel: 21cm image at $z = 7.02$ as derived from a full numerical simulation of reionization (XL2 from Iliev et al. 2014), convolved with a 5 arcminute FWHM Gaussian beam and 0.8 MHz bandwidth. The dark parts are large ionized regions. Right panel: a constructed 21cm signal with the same power spectrum as the signal in the left panel but a Gaussian PDF. These two images are very different but indistinguishable in a statistical power spectrum analysis.

with x_{HI} the neutral hydrogen fraction, $\delta = \rho/\langle \rho \rangle - 1$, the overdensity in the baryon distribution, T_s the spin (or excitation) temperature of the 21cm transition, $T_{CMB}(z)$ the Cosmic Microwave Background (CMB) temperature, z the redshift of the signal, Ω_m and Ω_b, the total matter and baryon density in terms of the critical density, h the Hubble parameter in units of $100 \, \text{km s}^{-1} \, \text{Mpc}^{-1}$, Y_p the primordial helium abundance by mass, and $dv_\parallel/dr_\parallel$ the proper gradient of the peculiar velocity along the line of sight. This last term represents the effect of redshift space distortions.

From this expression one sees that the 21cm signal varies with position due to variations in the matter overdensity δ, the hydrogen neutral fraction x_{HI}, the spin temperature T_S and line of sight velocity gradient $dv_\parallel/dr_\parallel$. This forms the basis of the analysis of the 21cm signal be it statistically or tomographically.

3. Regimes for Imaging

Imaging becomes possible once the signal to noise (S/N) for a certain size of spatial/spectral resolution element becomes larger than 1. Since the instrument noise will decrease when forming larger and larger resolution elements, even the first generation experiments such as LOFAR can in principle produce images, although with very poor resolution. This was worked out in detail in Zaroubi et al. (2012) where it was shown that LOFAR could produce images with a resolution of $\sim 20'$, whereas power spectrum analysis should be able to reach angular scales of $\sim 3'$.

Since the sensitivity of SKA1-Low varies with frequency, imaging will not be possible on the same scales at all frequencies. Specifically, as the sensitivity drops rapidly below the critical frequency the imaging capabilities for $\nu < 100$ MHz quickly deteriorate. In this regime larger image resolution elements will need to be used to reach the same noise levels. For those regimes in which imaging becomes unfeasible, statistical analysis with power spectra should be used.

3
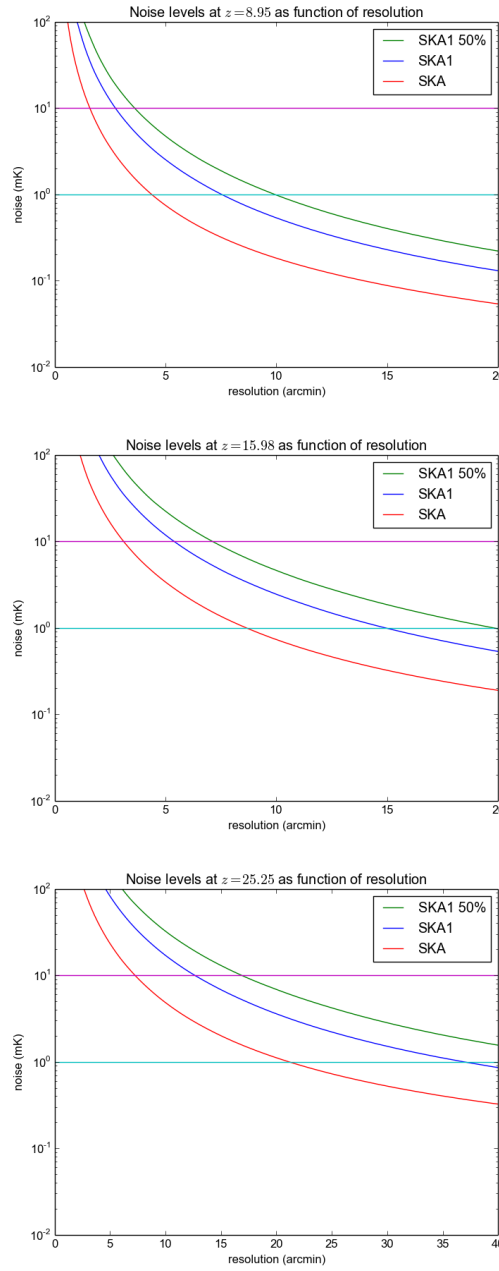
Figure 2: SKA-Low image noise levels as a function of imaging resolution for redshifts 8.95, 15.98 and 25.25. The assumed integration time is 1000 hrs and the frequency bandwidth is matched to the angular resolution. The different curves indicate the early science SKA1-Low, the full SKA1-Low and the final SKA2-Low. The horizontal lines are placed at 1 mK and 10 mK noise levels. These results can also be found in Koopmans & et al. (2015). The SKA1-Low configuration assumed is identical to the Baseline Design (Dewdney et al. 2013). Early science has half and the full SKA2-Low has four times the collecting area.

The three panels of Figure 2 illustrate the imaging capabilities of SKA-Low in three different stages: an early science 50% of the Baseline Design, the Baseline Design SKA1-Low (Dewdney

et al. 2013) and the full SKA2-Low at 4 times the sensitivity of SKA1-Low. All cases are for an integration time of 1000 hours and for a frequency bandwidth matched to the angular resolution. For tomography it is better if the frequency bandwidth matches the imaging scale so as to have fairly uniform resolution across the three-dimensional volume.

Concentrating on the full SKA1-Low case the figure shows that for $\nu \sim 140$ MHz ($z \sim 9$) imaging on scales down to $7'$ (19 comoving Mpc[1]) gives 1 mK noise levels. For the regime around 80 MHz this increases to scales of around $15'$ (47 cMpc) and only very coarse imaging at scales of 0.5 degree (100 cMpc) or worse is feasable for the lowest frequencies.

At noise levels of 1 mK it is possible to detect fluctuations in the neutral HI distribution. However, inspection of Eq. 2.1 shows that much larger amplitude variations can occur in the signal. For example, for the case of $T_s \gg T_{\mathrm{CMB}}$ the contrast between fully ionized and fully neutral regions at mean density is given by

$$27 \left(\frac{1+z}{10} \right)^{\frac{1}{2}} \quad \mathrm{mK}, \tag{3.1}$$

which should be detectable at higher noise levels than 1 mK. It is thus possible to map out the shapes of ionized regions at higher resolution. Figure 2 shows that for 10 mK noise, SKA1-Low could image ionized regions at $\sim 4'$ (11 cMpc) at $z \sim 9$.

Similarly, variations in the spin temperature during the Cosmic Dawn can result in more than 100 mK variations as can be seen from evaluating

$$27 \left(1 - \frac{T_{\mathrm{CMB}}(z)}{T_s} \right) \left(\frac{1+z}{10} \right)^{\frac{1}{2}} \quad \mathrm{mK}. \tag{3.2}$$

for T_s in the range 5 to 200 K. As can be seen from Figure 2 10 mK noise levels permit imaging with SKA1-Low at $\sim 6'$ (19 cMpc) scales around $z \sim 16$ and at $\sim 14'$ (47 cMpc) scales around $z \sim 25$.

For the other two configurations, the 50% SKA1-Low case requires roughly a 50% worse resolution and the SKA2-Low case allows roughly a factor 2 better resolution for the same noise levels, see Fig. 2.

To further illustrate the imaging capabilities of SKA1-Low, Figure 3 shows the result of an imaging pipeline in which an input image from a large scale reionization simulation has been observed by an interferometer with the same specifications as in the SKA1-Low Base Line Design (Dewdney et al. 2013) for 1000 hours. This pipeline is based on the MeqTrees software (Noordam & Smirnov 2010). The largest HII regions in this image are clearly visible (Shukla et al., in preparation).

4. Analyzing images

Once a tomographic data set has been obtained, it requires analysis to draw quantitative conclusions about the (astro)physics of the CD/EoR. Relying on the results of simulations several

---

[1]For these conversions the cosmological parameters from Eq. 2.1 are used.

[2]For computational reasons only 10% of the stations are used. To mimic the full SKA1-Low the noise is scaled down by a factor 10.
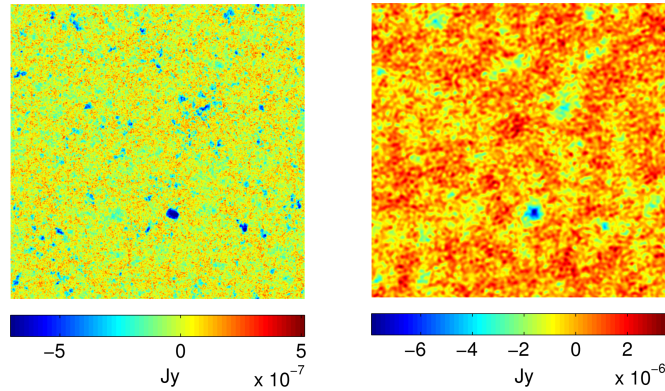
Figure 3: Left panel: The 21cm signal from a simulation of reionization in a 425 h^{-1} Mpc volume (Iliev et al. 2014). The redshift is $z = 8.515$ and it is assumed that $T_s \gg T_{CMB}$. The field is 3.64×3.64 degrees on the sky. Right panel: the 21cm signal plus thermal noise when observed with SKA1-Low for 1000 hours.[2] The frequency is 150 Mhz, bandwidth 1 MHz and only baselines less than 2 km are used. This gives a synthesized beam of $3.7' \times 3.2'$. The large HII region in the lower half of the image is 18.55 h^{-1} Mpc or 9.5' in size and is clearly recovered in the observed image.

methods have been considered for analyzing such three-dimensional data sets. However, as the focus of the SKA precursors is on statistical measurements, the analysis of tomographic data is still very much a field in development. In this section, we summarize some of the techniques that can be used. Section 5 provides an overview of the science that can be done with tomographic data.

4.1 Regions around special objects

By targeting a region which contains a special object, such as a bright quasar or a group of bright galaxies, the 21cm signal shows how this object has influenced its environment, either through its ionizing radiation, or through its heating. The measurement would provide the size and geometry of features in the 21cm signal (e.g. a spherical HII region around a bright quasar). Such measurements would presumably employ rather ad hoc analysis methods motivated by the interest in a specific area.

For the cases when the S/N is insufficient for imaging, for example when the HII region is small or during the Cosmic Dawn when the noise is high, a matched filter based method can be used to optimally detect such regions using the visibilities directly, although this does require making assumptions about the shape of the region. This can then be used to estimate their sizes (Datta et al. 2007, 2008). Another technique that can be applied in the low S/N case is the stacking of observations of several (similar) objects.

4.2 Bubble size measures

When not considering a special region, some sort of statistic is needed to characterize the tomographic data set. For example, one might want to characterize the distribution of HII bubble sizes. Although this sounds quite straightforward, in reality this will not be so. The reason for this is that the geometry of ionized sources is unlikely to be a set of isolated nearly spherical bubbles of various sizes. Simulations show that rather there exists a complex network of ionized regions which partly overlap. The reason for this is that the sources of reionization live in the developing

cosmic web and thus are spread out like beads on connected strings. Simple two-dimensional cuts through this geometry do not do justice to its complexity.

Several methods to characterize bubble sizes in simulation results have been suggested. These include the "spherical average method" (Zahn et al. 2007), the power spectra of the ionized fraction P_{xx}, the Friends-of-Friends (FoF) method (Iliev et al. 2006) and PDFs (probability distribution functions) of path lengths through ionized regions (Mesinger & Furlanetto 2007; Hong et al. 2014). The results of the first three methods were compared in Friedrich et al. (2011). The conclusion was that each method measures different aspects and depending on what one is after, each provides a useful measurement of bubble sizes.

It has to be noted that all of these methods rely on the ionized or neutral fraction to characterize the bubble size distribution. The use of these or similar methods on the redshifted 21cm signal from an interferometer requires more investigation as the presence of density fluctuations, noise, synthesized beam shape and possibly residual foregrounds will affect their results.

4.3 Topological measures

A different property of the distribution of ionized regions is their geometry and topology. These are often described through the so-called Minkowski Functionals which provide the total volume, total surface, mean curvature and the so-called Euler Characteristic χ. The latter is a number characterizing the topology of the regions, sometimes also expressed as the *genus g*, where $g = 1 - \chi$. If N_{part} is the total number of isolated regions, N_{tunnel} the number of tunnels through these regions and N_{cavity} the number of cavities inside these regions, then

$$\chi = N_{part} - N_{tunnel} + N_{cavity} \tag{4.1}$$

The work in Gleser et al. (2006); Lee et al. (2008); Friedrich et al. (2011); Hong et al. (2014) suggests that such topological measurements will be useful to characterize the reionization process and distinguish between different models. However, as for the bubble size methods discussed above, also here more work is needed to adapt these methods for use with real 21cm data.

4.4 Effects of finite resolution

Interferometers have both a minimum and maximum scale for which they are sensitive and this will impact the images. Starting with the minimum scale, finite resolution will limit the interpretation of the data. Fluctuations in density, neutral fraction and spin temperature below the resolution scale will not be separable. This means for example that a resolution element with a low value of the 21cm signal can be either a low density region or a high density region with several small, unresolved HII regions.

However, tomography does offer the possibility of analyzing this further by creating an ionization mask. Large ionized regions should be easily identifiable from their uniform, low flux level. Masking these out from a statistical analysis, one can then derive power spectra for the 'neutral' regions. These regions will still contain unresolved effects from small HII regions but comparing power spectra from different redshifts would allow detecting their effects on the density field. Note that such a masked analysis of the density field is only possible with tomographic data supplying the location of the masks.

As is well known, interferometers do not have baselines with zero separation and thus are unable to measure the average value of the signal within the FoV. In fact, there is a range of angular scales that cannot be measured, determined by the length of the smallest baseline. The smallest baseline for SKA1-Low has not yet been defined but will presumably lie in the range of ∼30 m implying that modes on scales of more than a few degrees will not be contained in the tomographic data. It is therefore important that these missing scales do not contain astrophysically or cosmologically essential structures as it would be impossible to reliably reconstruct these from the observations. Since we expect such information up to scales of a few degrees, shortest baselines of ∼30 m are required for the CD/EoR science case (Mellema et al. 2013). This implies station sizes of at least this size, although the availability of correlations between individual dipoles within stations would make it possible to capture even larger scales.

5. Science from images

In this section we discuss briefly some of the questions about Reionization and the Cosmic Dawn that can be answered by analysing the tomographic 21cm signal. Please also see Wyithe et al. (2015) in this volume for a case study of imaging with SKA1-Low.

5.1 QSO properties

By mapping out the shape of the ionized region around a bright quasar several properties of the quasar can be derived. A requirement for this is that the ionizing photon production from quasar dominates over the that of the local galaxy population. As quasars presumably live in biased, high density regions, this requirement is not trivially fulfilled. However, for optimistic assumptions about the radiation flux from a quasar, Datta et al. (2012) do find that a quasar can leave a clear imprint on its local environment.

As they are expected to be large and prominent features in the redshifted 21cm sky, the literature on quasar HII region in 21cm data is extensive (Wyithe et al. 2005; Geil & Wyithe 2008; Wyithe 2008; Furlanetto et al. 2008; Datta et al. 2012; Majumdar et al. 2012; Feng et al. 2013). The size of HII regions around the quasar can be used to put constraints on the quasar life time and luminosity, and possibly the mean neutral fraction of the surrounding IGM. The occurence of fossil HII regions will put constraints on the quasar population at high redshifts and will also measure the properties of the ionized IGM.

A growing quasar HII region that is spherical in shape in the quasar's rest frame, would appear to be distorted ('egg-shaped') along the line of sight in a tomographic data set due to the light cone effect (Shapiro & Giroux 1987; White et al. 2003; Wyithe & Loeb 2004; Yu 2005). From this apparent anisotropy of its shape, constraints on the quasar's ionizing luminosity, its age and neutral fraction of the local IGM can be derived (Geil & Wyithe 2008; Majumdar et al. 2012)[3] The constraints obtained from tomographic data will be more stringent than the ones currently avialable from the quasar absorption spectra (e.g. Bolton et al. 2011).

---

[3]We note that besides tomographic imaging the same can be achieved using an improved matched filter technique (Majumdar et al. 2012) acting directly on the actual visibilities. This will possibly provide a better handle on the noise than the image cube (Datta et al. 2007; Malloy & Lidz 2013) although the choice of the filter shape is important.

In addition such measurements will allow us to measure the possible anisotropy of the emission from the quasar itself. If the ionizing radiation only escapes in certain directions due to the presence of an obscuring torus, as is seen in many lower redshift quasars, the imprint on the surrounding medium will not be spherical. If such an anisotropy would be found in the 21cm data, it would be the first three-dimensional mapping of the radiative anisotropy of a high redshift active galactic nucleus.

If quasars are present during the Cosmic Dawn, heating of the surrounding IGM by their X-ray flux could leave strong imprints on the 21cm signal, creating 21cm emission regions against a background of absorption. The contrast between the absorption and emission regions could be as high as 200 mK which would make it possible to image these even at quite high redshifts (Alvarez et al. 2010), see also section 5.6 below.

5.2 Connection between galaxy population and HII regions

Determining the volume and shape of the ionized region around a group of optically detected galaxies would allow one to infer the connection between the ionizing radiation output of a galaxy population and the brightest members of this population. It is well-known that the galaxies we can currently detect are insufficient to reionize the Universe (see e.g. Schmidt et al. 2014) and references therein). However, the shape and extent of the luminosity function for the unobserved population remains a matter of contention. By measuring the specific examples of known galaxy groups, better constraints on this problem can be derived. In addition such observations would map the developing cosmic web.

As far as we know, no systematic exploration of such an approach has been performed. Most of the work connecting galaxies and the 21cm signal has focused on performing a cross-correlation between a galaxy survey and a 21cm observation. This technique can even be employed in noise regimes where imaging is not possible (Furlanetto & Lidz 2007; Wyithe & Loeb 2007; Lidz et al. 2009; Wiersma et al. 2013; Park et al. 2014).

5.3 Bubble size distribution & topology - breaking degeneracies in reionization models.

Although power spectrum analysis will be an important tool to determine the parameters of reionization, it can be expected that there will be certain degeneracies between key parameters. As the 21cm signal has a non-Gaussian distribution, power spectra do not fully describe it and quite different models could be consistent with the same power spectrum. It is likely although not proven that tomographic data can break some of the degeneracies in a pure power spectrum analysis.

Both from the point of view of cosmology and galaxy evolution, the important question is how to connect the measured size distribution of HII regions to the dark matter halo distribution. This correspondence will not be trivial as it involves a range of (astro)physical processes, such as the feedback (thermal, mechanical etc), recombinations etc. The measured bubble size distribution and topology will shed light on all these mechanisms. However, to date a detailed study of how to reliably extract this information from such measurements remains to be done.

5.4 Measurements of the cosmological density field

As explained in Section 4.4, knowing the location of large ionized regions would allow excluding these from the analysis of the remaining signal, which would then be a modified version

of the cosmological density field. Since reionization is likely to occur earlier in denser regions, the remaining signal would be dominated by lower density regions and affected by unresolved ionized regions. Still, a measurement such as this would provide useful information, especially if complemented by higher redshift power spectrum measurements. However, in order to produce high quality masks and to detect significant density fluctuations, high resolution is required. Likely this application will only become feasible with the full SKA2-Low[4].

5.5 Measuring the global 21cm signal

Since the intrinsic signal from the ionized regions will be zero or at least very close to zero, the presence of well resolved ionized regions could be used as a zero-point to determine the power contained in scales above those set by the minimum baseline of the interferometer, $> 3°$ (at 150 MHz) for SKA-Low. We do not expect substantial power in the spectrum of 21cm fluctuations beyond these scales and consequently the value will be nearly equal to the mean 21cm signal in the Universe at that epoch. Measuring the flux from well-resolved HII regions will thus yield an independent measurement of the global 21cm signal. This technique does rely on the presence of large enough ionized regions with mininal contribution from unresolved neutral structures within them. A similar constant 'zero-point' could possibly also be found during the Cosmic Dawn if one assumes that the regions with the lowest signal are the coldest ones whose temperature can be derived from adiabatic cooling due to the expansion of the Universe.

5.6 Cosmic Dawn Science

Before $z \sim 12$, the spatial variations in the 21cm signal are expected to be mostly due to variations in the spin temperature. As explained in Section 3, cold regions could generate high amplitude signals (> 100 mK). Therefore higher image noise levels of $10 - 30$ mK are acceptable, allowing for higher resolution images at these frequencies. The spin temperature evolution is thought to have two phases, an initial one during which UV photons from the first stars will decouple the spin temperature from the CMB temperature and couple it to the (cold) gas kinetic temperature, thus making the 21 cm signal observable against the background CMB. This phase is followed by a phase in which the cold IGM will be heated by X-ray radiation, turning the 21cm signal from absorption into emission. Both phases will likely be patchy and thus excellent targets for tomography (see e.g. Mesinger et al. 2014)).

To start with the heating phase, the heating profile and the 21 cm signal around X-ray sources will depend strongly on the flux and spectrum of the X-ray radiation reaching the IGM. This in its turn will depend on the intrinsic X-ray flux and spectrum and the level of absorption within the host galaxies. For mini-QSOs or a hot interstellar medium in star-forming galaxies, which emit substaintial amounts of soft X-ray (< 1 Kev) photons, heated regions will be smaller and the heating will be patchy (Pacucci et al. 2014; Ghara et al. 2014). On the other hand, heating will be more homogeneous and heated regions will be very large if the spectrum is dominated by hard X-ray photons, for example in the case of high mass X-ray binaries (Fialkov et al. 2014) and/or a

---

[4]We note that an alternative way to probe the large scale density distribution is to measure the dark matter power spectrum. It has been proposed that anisotropies in the HI 21 cm power spectra arising from the peculiar velocities ('redshift space distortions') can be used to extract the 'pure' dark matter power spectrum from the astrophysical HI power spectra (Barkana & Loeb 2005; Shapiro et al. 2013).

high level of absorption within the host galaxies. Thus the measurement of sizes of heated regions will be a direct probe of the first X-ray sources and their spectra. This measurement will also probe the level of the X-ray background (Christian & Loeb 2013; Mesinger et al. 2014).

During the earlier decoupling phase the patchiness is driven by the rarity and clustering of the sources of UV photons. Even though this phase is expected around $z \sim 20$, the decoupled regions around these sources may still be imaged with SKA-Low as the contrast between coupled and decoupled regions will be high (~ 100 mK, see for example Semelin et al. 2007; Santos et al. 2008; Mesinger et al. 2014; Ghara et al. 2014). Measurements of size and distribution of the decoupled regions would probe the nature of the very first stars and their environment.

One particularly interesting application of tomography for the early Cosmic Dawn would be to map out the effects of 'bulk flows', an expected large scale variation of the velocity difference between dark and baryonic matter (Tseliakhovich & Hirata 2010). This effect would modulate early star formation on scales of ~ 100 Mpc, corresponding to $30'$ at $z = 20$. Both the modulation in the UV background and the heating could generate observable signatures (McQuinn & O'Leary 2012). In spite of the low sensitivity for imaging around 65 MHz, such a modulation would actually fall within the imaging possibilities of SKA-Low.

It should be pointed out that most of the papers cited above focus on power spectrum analysis of the 21cm signal from the Cosmic Dawn. More work is needed to establish the impact of different kinds of X-ray and UV sources on the 21cm signal and how well these phenomena could be imaged with SKA-Low.

6. Conclusions

SKA-Low will transform the study of the Cosmic Dawn and the Epoch of Reionization by allowing tomographic imaging of the 21cm signal. With this capability we will be able to address a range of questions not accessible to a statistical, power spectrum characterization of the signal. Deep observations of 1000 hours with SKA1-Low will provide ~ 1 mK image noise levels at resolutions ranging from $\sim 7'$ at ~ 200 MHz to $\sim 30'$ at ~ 50 MHz, assuming a frequency bandwidth matching in physical size. However, many features such as isolated ionized regions during the EoR and isolated heated regions during the CD, can be imaged at ~ 10 mK noise levels, allowing image resolution elements in the range $4' - 14'$ in the same frequency range.

Tomographic imaging will allow the characterization of individual bright quasars, including their isotropy or lack thereof. It will also make it possible to connect the 21cm observations to optical galaxy surveys, thus unravelling the connection between photon producing galaxies and the reionization process. The ionized bubble size distribution and the topology of ionized regions uniquely characterize the reionization process. Extracting these from the observations requires tomographic imaging as they are not described by the power spectrum of the 21cm signal, due to its inherent non-Gaussian signature. Furthermore, identifying the location of ionized regions will make it possible to study the baryonic density field during reionization and using the ionized regions as a zero-point can be used to determine the global 21cm signal. Tomographic imaging thus opens the door to a wide range of studies inaccessible to a power spectrum analysis and essential to understand the reionization process.

The relatively coarse imaging possible for the highest redshifts may still be able to characterize the sizes and distribution of 'heated' and 'decoupled' regions and the effect of the velocity differences between dark matter and baryonic matter during the Cosmic Dawn. This will provide a unique and important probe of the very first X-ray and UV sources.

None of the existing low frequency precursors is capable of tomographically imaging the redshifted 21cm signal and even the planned HERA project will only attempt imaging at very large scales and during the EoR. This makes SKA-Low in all its phases a truly transformational telescope which will not only provide detailed 3D tomographic imaging of the EoR but also coarse, yet groundbraking imaging of the Cosmic Dawn. SKA-Low will be the only telescope on Earth capable of looking this far back in the history of our Universe and reveal the earliest phases of star and galaxy formation.

References

Alvarez, M. A., Pen, U.-L., & Chang, T.-C. 2010, ApJ, 723, L17

Barkana, R., & Loeb, A. 2005, ApJ, 624, L65

Bolton, J. S., Haehnelt, M. G., Warren, S. J., et al. 2011, MNRAS, 416, L70

Christian, P., & Loeb, A. 2013, JCAP, 9, 14

Datta, K. K., Bharadwaj, S., & Choudhury, T. R. 2007, MNRAS, 382, 809

Datta, K. K., Friedrich, M. M., Mellema, G., Iliev, I. T., & Shapiro, P. R. 2012, MNRAS, 424, 762

Datta, K. K., Majumdar, S., Bharadwaj, S., & Choudhury, T. R. 2008, MNRAS, 391, 1900

Dewdney, P., Turner, W., Millenaar, R., McCool, R. Lazio, J., & Cornwell, T. 2013, SKA1 System Baseline Design, Document number SKA–TEL–SKO–DD–001 Revision 1

Feng, Y., Croft, R. A. C., Di Matteo, T., & Khandai, N. 2013, MNRAS, 429, 1554

Fialkov, A., Barkana, R., & Visbal, E. 2014, Nature, 506, 197

Friedrich, M. M., Mellema, G., Alvarez, M. A., Shapiro, P. R., & Iliev, I. T. 2011, MNRAS, 413, 1353

Furlanetto, S. R., Haiman, Z., & Oh, S. P. 2008, ApJ, 686, 25

Furlanetto, S. R., & Lidz, A. 2007, ApJ, 660, 1030

Furlanetto, S. R., Oh, S. P., & Briggs, F. H. 2006, Phys. Rep., 433, 181

Geil, P. M., & Wyithe, J. S. B. 2008, MNRAS, 386, 1683

Ghara, R., Choudhury, T. R., & Datta, K. K. 2014, ArXiv:1406.4157, arXiv:1406.4157

Gleser, L., Nusser, A., Ciardi, B., & Desjacques, V. 2006, MNRAS, 370, 1329

Hong, S. E., S.Ahn, K., Park, C., et al. 2014, Journal of Korean Astronomical Society, 47, 49

Iliev, I. T., Mellema, G., Ahn, K., et al. 2014, MNRAS, 439, 725

Iliev, I. T., Mellema, G., Pen, U.-L., et al. 2006, MNRAS, 369, 1625

Koopmans, L. V. E., & et al. 2015, in Advancing Astrophysics with the Square Kilometre Array (Proceedings of Science), PoS(AASKA14)001

Lee, K.-G., Cen, R., Gott, III, J. R., & Trac, H. 2008, ApJ, 675, 8

Lidz, A., Zahn, O., Furlanetto, S. R., et al. 2009, ApJ, 690, 252

Madau, P., Meiksin, A., & Rees, M. J. 1997, ApJ, 475, 429

Majumdar, S., Bharadwaj, S., & Choudhury, T. R. 2012, MNRAS, 426, 3178

Malloy, M., & Lidz, A. 2013, ApJ, 767, 68

McQuinn, M., & O'Leary, R. M. 2012, ApJ, 760, 3

Mellema, G., Iliev, I. T., Pen, U.-L., & Shapiro, P. R. 2006, MNRAS, 372, 679

Mellema, G., Koopmans, L. V. E., Abdalla, F. A., et al. 2013, Experimental Astronomy, 36, 235

Mesinger, A., Ewall-Wice, A., & Hewitt, J. 2014, MNRAS, 439, 3262

Mesinger, A., & Furlanetto, S. 2007, ApJ, 669, 663

Noordam, J. E., & Smirnov, O. M. 2010, A&A, 524, A61

Pacucci, F., Mesinger, A., Mineo, S., & Ferrara, A. 2014, MNRAS, 443, 678

Park, J., Kim, H.-S., Wyithe, J. S. B., & Lacey, C. G. 2014, MNRAS, 438, 2474

Santos, M. G., Amblard, A., Pritchard, J., et al. 2008, ApJ, 689, 1

Schmidt, K. B., Treu, T., Trenti, M., et al. 2014, ApJ, 786, 57

Semelin, B., Combes, F., & Baek, S. 2007, A&A, 474, 365

Shapiro, P. R., & Giroux, M. L. 1987, ApJ, 321, L107

Shapiro, P. R., Mao, Y., Iliev, I. T., et al. 2013, Physical Review Letters, 110, 151301

Tseliakhovich, D., & Hirata, C. 2010, Phys. Rev. D, 82, 083520

White, R. L., Becker, R. H., Fan, X., & Strauss, M. A. 2003, AJ, 126, 1

Wiersma, R. P. C., Ciardi, B., Thomas, R. M., et al. 2013, MNRAS, 432, 2615

Wyithe, J. S. B. 2008, MNRAS, 387, 469

Wyithe, J. S. B., Geil, P. M., & Kim, H. 2015, in Advancing Astrophysics with the Square Kilometre Array (Proceedings of Science), PoS(AASKA14)015

Wyithe, J. S. B., & Loeb, A. 2004, ApJ, 610, 117

—. 2007, MNRAS, 375, 1034

Wyithe, J. S. B., Loeb, A., & Barnes, D. G. 2005, ApJ, 634, 715

Yu, Q. 2005, ApJ, 623, 683

Zahn, O., Lidz, A., McQuinn, M., et al. 2007, ApJ, 654, 12

Zaroubi, S., de Bruyn, A. G., Harker, G., et al. 2012, MNRAS, 425, 2964